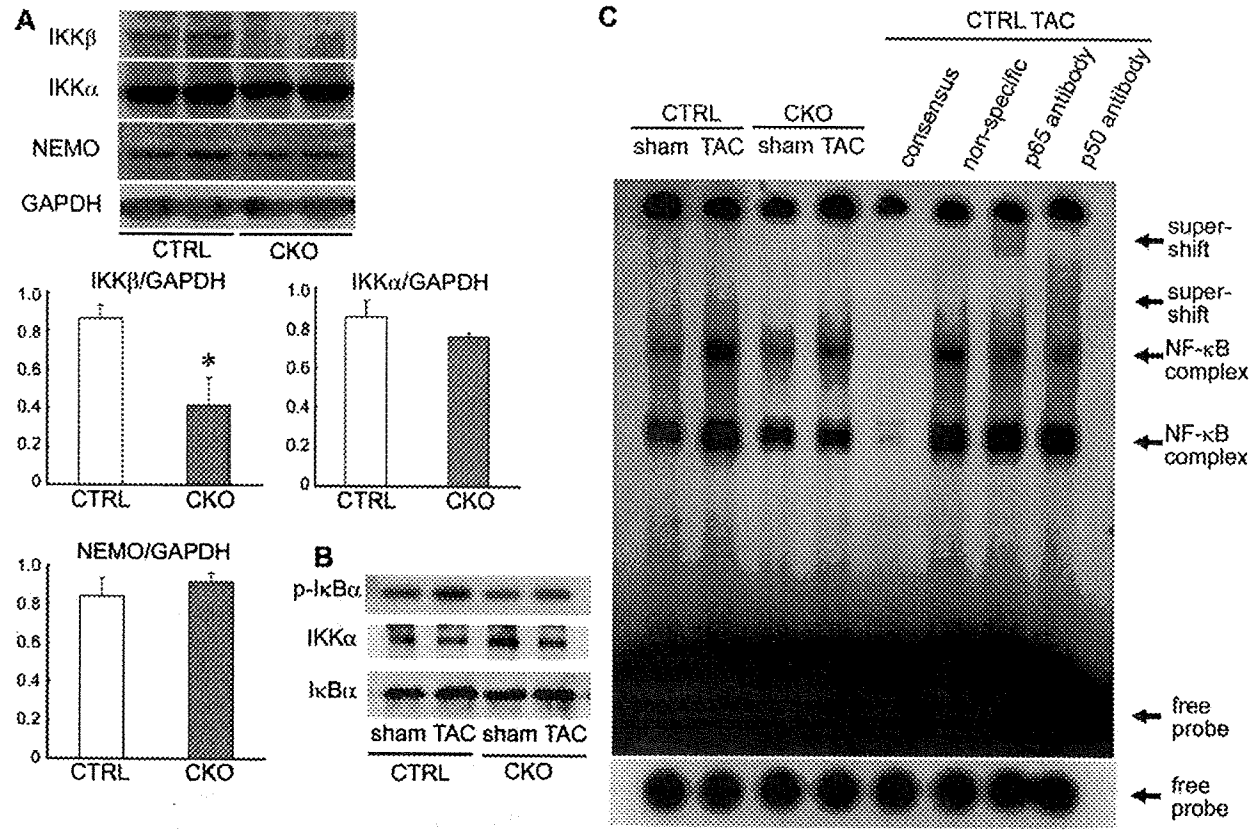

Figure 1. Characterization of cardiac-specific IKKβ-deficient mice. A, Western blot analysis of IKK complex components using homogenates from 10-week-old CTRL or CKO hearts, as well as the densitometric analysis of those blots. B, IKK kinase assay using homogenates from CTRL or CKO hearts 2 days after TAC. IKKα is shown as loading control. IκBα was used as a substrate. C, EMSA using nuclear proteins from CTRL or CKO hearts 2 days after TAC.

Generation of Cardiac-Specific IKKβ-Deficient Mice

To investigate the in vivo role of IKK/NF-κB activation in response to pressure overload, we generated cardiac-specific IKKβ-deficient mice. We crossed *Ikbkβ* $^{flox/flox}$ mice[12] with *MLC2V-Cre* mice to generate *Ikbkβ* $^{flox/flox}$;*MLC2V-Cre*$^{+}$ mice (CKO). We used *Ikbkβ* $^{flox/flox}$;*MLC2V-Cre*$^{-}$ littermates as controls (CTRL). Immunoblot analysis of hearts from 10-week-old mice indicated an ≈60% reduction in IKKβ protein level in CKO hearts relative to protein expression in CTRL hearts (Figure 1A). There were no differences in the expression levels of other IKK complex components such as IKKα and NEMO between CKO and CTRL (Figure 1A).

Normal Cardiac Structure and Function in IKKβ-Deficient Mice

The CTRL and CKO mice were born at the expected mendelian ratios (n=76 and 77, respectively). The CKO mice were normal at birth, and their external appearance was indistinguishable from that of their CTRL littermates. The mice grew to adulthood and were fertile. There was no difference in survival at 1 year between CTRL and CKO. Thus, IKKβ is not essential for cardiac development in mice.

The CKO hearts showed no evidence of cardiac morphological defects. Histological examination of the hearts from 10-week-old mice demonstrated no myofibrillar disarray, necrosis, or ventricular fibrosis under basal conditions (data not shown). In addition, heart weight, hemodynamic data, and echocardiographic parameters (Tables 1 and 2) were not significantly different between CKO and CTRL. These findings indicate that CKO had normal global cardiac structure and function.

Table 1. Physiological Parameters Under Basal Conditions in Ten-Week-Old Mice

Parameter	CTRL (n=8)	CKO (n=6)
Body weight, g	27.30±0.45	27.54±0.58
Heart weight, mg	128.4±2.7	122.9±2.5
Tibia length, mm	17.47±0.16	17.36±0.09
HW/BW, mg/g	4.71±0.09	4.47±0.06
HW/tibia length, mg/mm	7.36±0.19	7.08±0.13
LVSP, mm Hg	94±4	88±6
LVEDP, mm Hg	4±1	4±1
dp/dt max, mm Hg/sec	7888±512	8067±634
dp/dt min, mm Hg/sec	−4438±436	−4183±444
Heart rate, bpm	305±19	315±23

HW/BW indicates heart weight/body weight ratio; LVSP, LV systolic pressure; LVEDP, LV end-diastolic pressure. The dp/dt_{max} and dp/dt_{min} are the maximal rates of pressure development during contraction and relaxation, respectively. Data are expressed as means±SEM. There were no significant differences between CTRL and CKO in all physiological parameters.

Table 2. Echocardiographic Parameters Under Basal Conditions in Ten-Week-Old Mice

Parameter	CTRL (n=10)	CKO (n=10)
IVSd, mm	0.78±0.02	0.73±0.02
LVPWd, mm	0.80±0.03	0.79±0.03
LVDd, mm	3.40±0.06	3.43±0.05
LVDs, mm	1.97±0.06	1.94±0.05
LVFS, %	42.0±1.0	43.4±0.8
Heart rate, bpm	596±9	601±8

IVSd indicates diastolic interventricular septum thickness; LVPWd, diastolic LV posterior wall thickness; LVDd, end-diastolic LV dimension; LVDs, end-systolic LV dimension; LVFS, LV fractional shortening. Data are expressed as means±SEM. There were no significant differences between CTRL and CKO in all echocardiographic parameters.

Development of Congestive Heart Failure in Response to Pressure Overload in IKKβ-Deficient Mice

We subjected 10-week-old CKO and CTRL to pressure overload by means of TAC. First, we examined whether pressure overload–induced IKK/NF-κB activation is efficiently inhibited in CKO hearts. Cytosolic and nuclear proteins were extracted from hearts 2 days after TAC and subjected to either in vitro kinase assay or EMSA (Figure 1B and 1C). TAC induced the activation of IKK and the formation of NF-κB–DNA complexes in CTRL after TAC. NF-κB activation was attenuated in CKO hearts. The specificity of NF-κB–binding activity was confirmed by the competition assay and supershift assay using anti-p50 and anti-p65 subunit antibodies. One week after TAC, we performed echocardiographic analysis (Figure 2A). The diastolic interventricular septum thickness and diastolic left ventricular (LV) posterior wall thickness were not significantly different between CKO and CTRL subjected to TAC (Figure 2B and 2C). One week after sham operation, the end-diastolic LV dimension and LV fractional shortening were not significantly different between CTRL and CKO. However, end-diastolic LV dimension was significantly elevated and LV fractional shortening had significantly reduced in TAC-operated CKO compared with both sham-operated CKO and TAC-operated CTRL (Figure 2D and 2E). Furthermore, the lung/body weight ratio, an index of lung congestion, was significantly elevated in TAC-operated CKO compared with the other groups (Figure 2F). Only 1 of 19 CKO mice died before 1 week after TAC, whereas all CTRL mice (n=15) lived up to 1 week after TAC. These findings indicate that CKO developed congestive heart failure in response to pressure overload.

Enhancement of Pressure Overload–Induced Cardiac Remodeling and Fibrosis in IKKβ-Deficient Mice

Although the ratio of heart weight/body weight was not significantly different between sham-operated groups 1 week after surgery, the ratio was significantly higher in TAC-operated CKO than TAC-operated CTRL (Figure 3A). TAC increased cardiomyocyte cross-sectional area in both CKO and CTRL (Figure 3B). However, cardiomyocyte cross-sectional area was significantly greater in TAC-operated CKO than in TAC-operated CTRL. We evaluated the level of atrial natriuretic factor (ANF) and brain natriuretic peptide

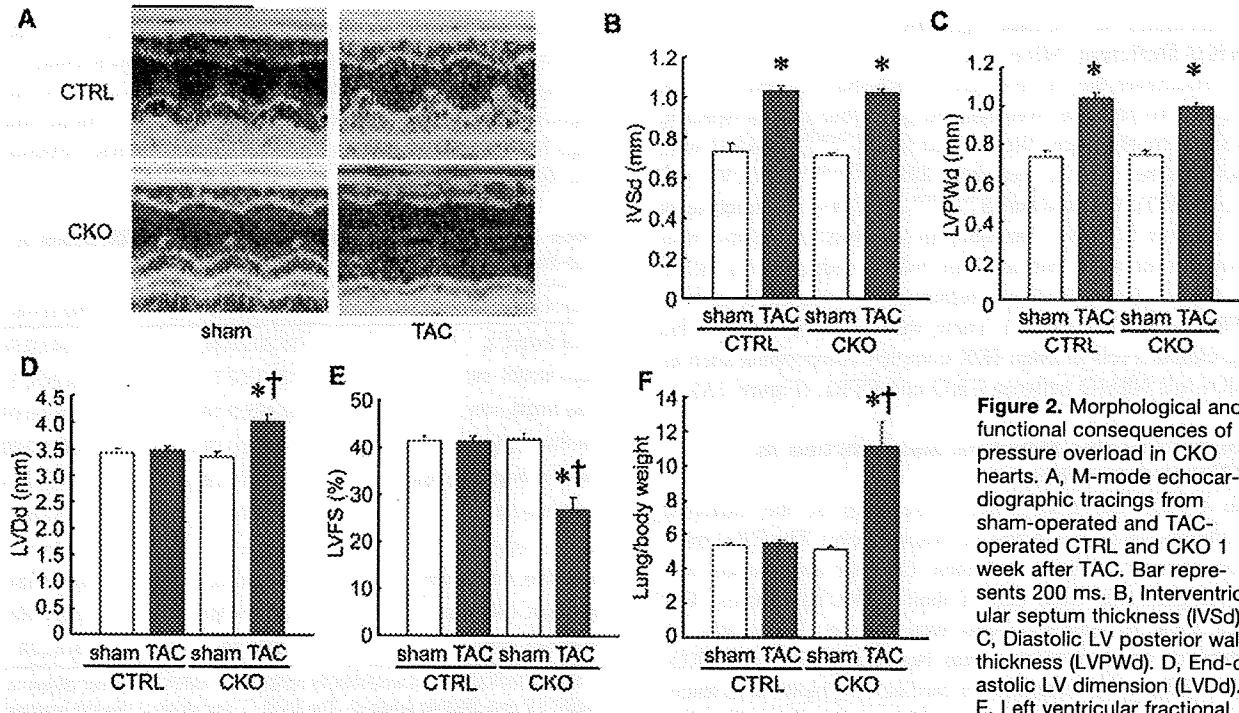

Figure 2. Morphological and functional consequences of pressure overload in CKO hearts. A, M-mode echocardiographic tracings from sham-operated and TAC-operated CTRL and CKO 1 week after TAC. Bar represents 200 ms. B, Interventricular septum thickness (IVSd). C, Diastolic LV posterior wall thickness (LVPWd). D, End-diastolic LV dimension (LVDd). E, Left ventricular fractional shortening (LVFS). F, Lung weight/body weight ratio 1 week after TAC. Sham-operated CTRL (n=8), TAC-operated CTRL (n=14), sham-operated CKO (n=7), TAC-operated CKO (n=14). *$P<0.05$ vs corresponding sham-operated mice; †$P<0.05$ vs TAC-operated CTRL.

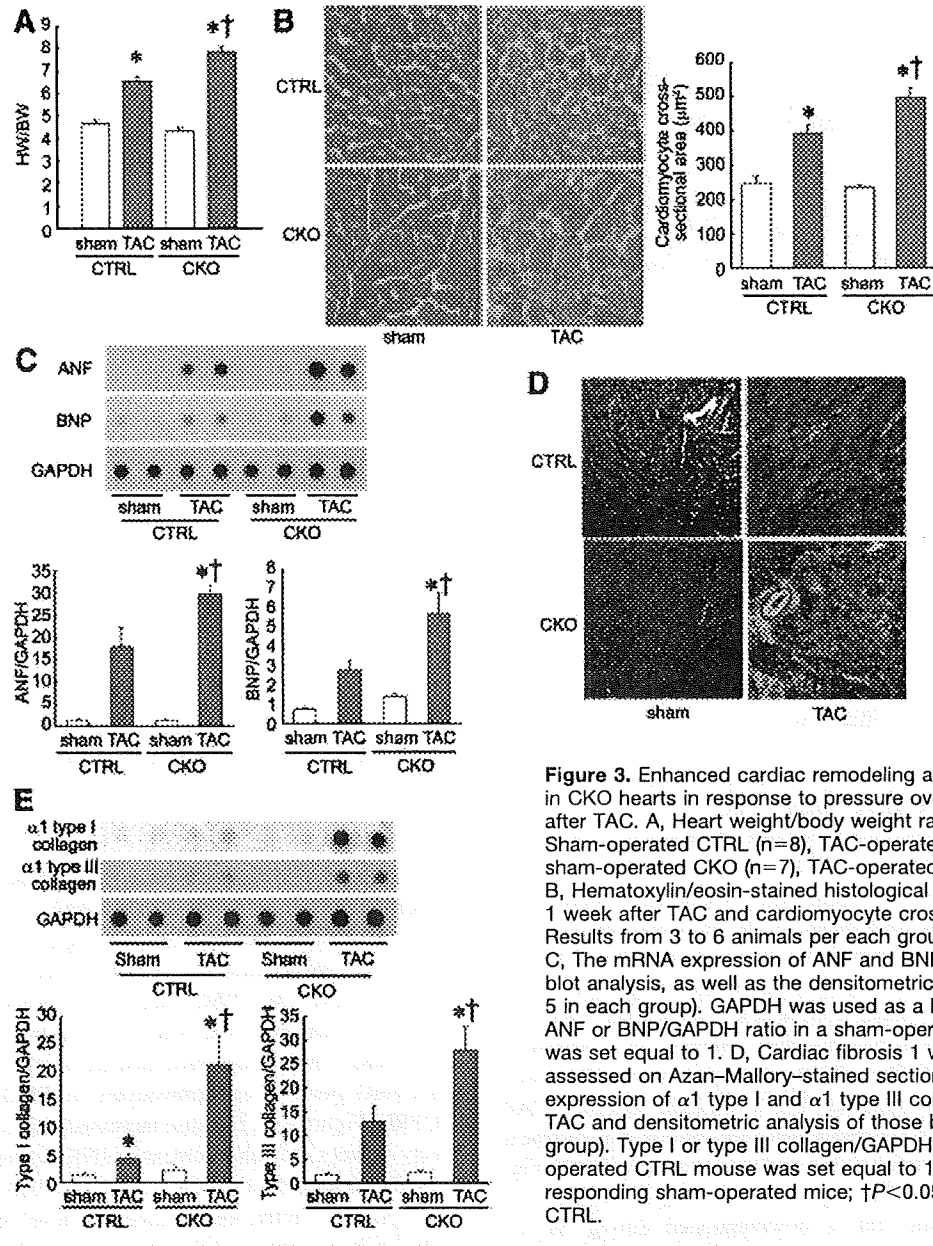

Figure 3. Enhanced cardiac remodeling and fibrotic change in CKO hearts in response to pressure overload 1 week after TAC. A, Heart weight/body weight ratio (HW/BW). Sham-operated CTRL (n=8), TAC-operated CTRL (n=14), sham-operated CKO (n=7), TAC-operated CKO (n=14). B, Hematoxylin/eosin-stained histological sections of hearts 1 week after TAC and cardiomyocyte cross-sectional area. Results from 3 to 6 animals per each group were included. C, The mRNA expression of ANF and BNP assessed by dot blot analysis, as well as the densitometric analysis (n=3 to 5 in each group). GAPDH was used as a loading control. ANF or BNP/GAPDH ratio in a sham-operated CTRL mouse was set equal to 1. D, Cardiac fibrosis 1 week after TAC assessed on Azan–Mallory–stained sections. E, mRNA expression of α1 type I and α1 type III collagen 1 week after TAC and densitometric analysis of those blots (n=3 in each group). Type I or type III collagen/GAPDH ratio in a sham-operated CTRL mouse was set equal to 1. *$P<0.05$ vs corresponding sham-operated mice; †$P<0.05$ vs TAC-operated CTRL.

(BNP) mRNA expression by means of dot blot analysis (Figure 3C). ANF and BNP, which are biochemical markers of cardiac remodeling, were not significantly different between sham-operated groups but were significantly higher in TAC-operated CKO than in TAC-operated CTRL. Two days after TAC, when LV function is similar in both groups, the extent of cardiac hypertrophy was not significantly different between CTRL and CKO (data not shown). These findings suggest that enhanced cardiac hypertrophy in CKO 1 week after TAC was secondary to LV dysfunction.

Azan–Mallory staining demonstrated that interstitial and perivascular fibrosis was present in both CTRL and CKO hearts after TAC, but the extent of fibrosis in CKO was much greater than in CTRL (Figure 3D). The induction of both α1 type I and type III collagen mRNA 1 week after TAC was significantly enhanced in CKO relative to expression in CTRL (Figure 3E).

Increased Cardiomyocyte Apoptosis in IKKβ-Deficient Mice

We evaluated cardiomyocyte apoptosis in hearts 1 week after TAC by means of an in situ TUNEL assay and immunohistochemical analysis using an anti–activated caspase 3 antibody. TUNEL-positive cells contained condensed chromatin and were identified as cardiomyocytes by anti–α-sarcomeric actin staining (Figure 4A). The numbers of TUNEL-positive cardiomyocytes in sham-operated CTRL and sham-operated CKO were similar. However, TAC-operated CKO exhibited more TUNEL-positive cardiomyocytes than TAC-operated CTRL. Although the number of activated caspase 3–positive cardiomyocytes 1 week after TAC was not significantly different between sham-operated CTRL and sham-operated CKO, it was significantly higher in TAC-operated CKO compared with TAC-operated CTRL (Figure 4B). These

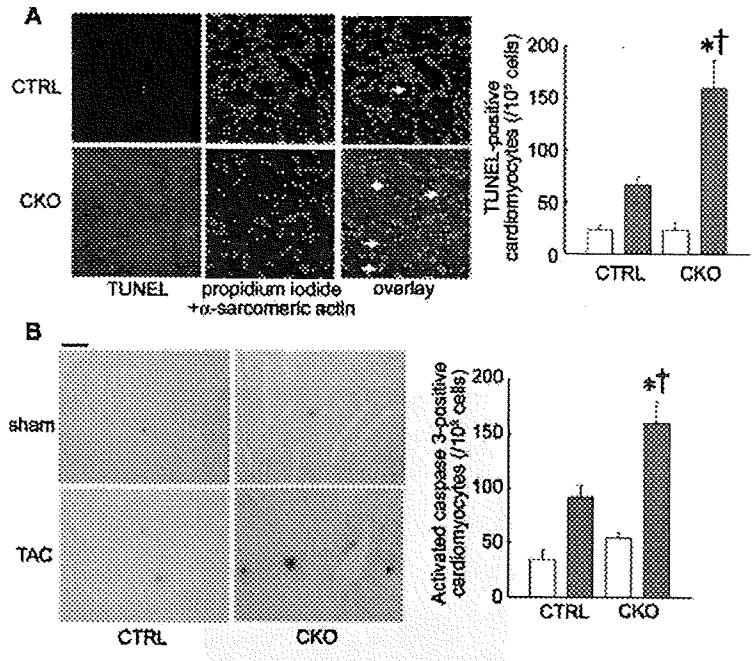

Figure 4. Evaluation of cardiomyocyte apoptosis in response to pressure overload. A, Triple staining of CTRL and CKO hearts with TUNEL, propidium iodide, and anti–α-sarcomeric actin antibody 1 week after TAC. White arrows indicate TUNEL-positive cardiomyocytes. The graph shows the number of TUNEL-positive cardiomyocytes 1 week after TAC (n=3 in each group) (right). Open and gray bars represent sham- and TAC-operated mice, respectively. B, Immunohistochemical analysis of CTRL and CKO hearts 1 week after TAC with anti–activated caspase 3 antibody. Bar represents 25 μm. The graph shows the number of activated caspase 3-positive cardiomyocytes 1 week after TAC (n=3 in each group) (right). Open and gray bars represent sham- and TAC-operated mice, respectively. *$P<0.05$ vs corresponding sham-operated mice; †$P<0.05$ vs TAC-operated CTRL.

findings suggest that increased apoptosis might be a cause of heart failure in CKO after TAC.

Downregulation of MnSOD Expression in IKKβ-Deficient Mice After TAC

Next, we investigated the molecular mechanism of increased apoptosis after TAC in CKO. We hypothesized that the impairment of NF-κB target gene expression induced by pressure overload contributes to the increased apoptosis in CKO. Thus, we examined the level of candidate NF-κB–target apoptosis–related genes expression 1 week after TAC. Total RNA was isolated from hearts 1 week after TAC and was subjected to either dot blot analysis or quantitative real-time RT-PCR. The mRNA expression levels of antiapoptotic molecules, such as Bfl-1, c-FLIP, Bcl-xl, XIAP TRAF2, c-IAP1, or Gadd45β, were not significantly different between TAC-operated CTRL and TAC-operated CKO (Figure 5A and 5B). The expression of Bnip3, which is a proapoptotic factor that is downregulated during NF-κB activation, was not significantly different between TAC-operated CTRL and TAC-operated CKO (Figure 5B). We also examined the expression levels of NF-κB–driven inflammatory cytokines. No significant differences in the expression level of TNF-α were detected among the 4 groups (Figure 5B). Expression of IL-1β tended to increase in TAC-operated groups. However, there were no significant differences between TAC-operated CKO and TAC-operated CTRL. IL-2 was not detected in the heart (data not shown).[2] Finally, we examined the expression of NF-κB–target antioxidative molecules, such as ferritin heavy chain and MnSOD. We did not detect any differences in ferritin heavy chain mRNA expression among groups (data not shown). MnSOD mRNA was significantly downregulated in TAC-operated groups compared with sham-operated groups. However, downregulation was significantly greater in TAC-operated CKO compared with TAC-operated CTRL (Figure 5C). Consistent with the levels of mRNA expression, protein expression was significantly lower in TAC-operated CKO compared with TAC-operated CTRL (Figure 5D). These findings suggest that enhanced downregulation of MnSOD might contribute to increased apoptosis after TAC in CKO.

Enhanced Oxidative Stress and JNK Activation in IKKβ-Deficient Mice After TAC

To investigate the pathophysiological consequences of MnSOD downregulation, we evaluated the extent of oxidative stress after TAC. Immunohistochemical staining of hearts 1 week after TAC with anti–8-hydroxy-deoxyguanosine (8-OHdG) antibody demonstrated an increase in the number of 8-OHdG–positive cardiomyocytes in CKO compared with CTRL (Figure 6A). Because increased oxidative stress reportedly induces the enhancement of JNK activity and cell death in NF-κB–deficient cells[19] and because JNK is a well-known proapoptotic factor, we examined the level of JNK phosphorylation in response to pressure overload. Although the phosphorylation level of p46 JNK was not significantly different between TAC-operated CTRL and TAC-operated CKO, the phosphorylation of p54 JNK was significantly higher in TAC-operated CKO compared with TAC-operated CTRL (Figure 6B). These findings suggest that enhanced oxidative stress and JNK activity mediated through downregulation of MnSOD might be involved in the increased apoptosis observed in CKO after TAC.

Attenuation of Isoproterenol-Induced Cardiomyocyte Death by Both a MnSOD Mimetic and a JNK Inhibitor in CKO

To confirm the involvement of MnSOD downregulation in the mechanism of increased cell death, we tested the effect of a MnSOD mimetic, MnTBAP, on isoproterenol-induced cardiomyocyte death. We isolated cardiomyocytes from adult

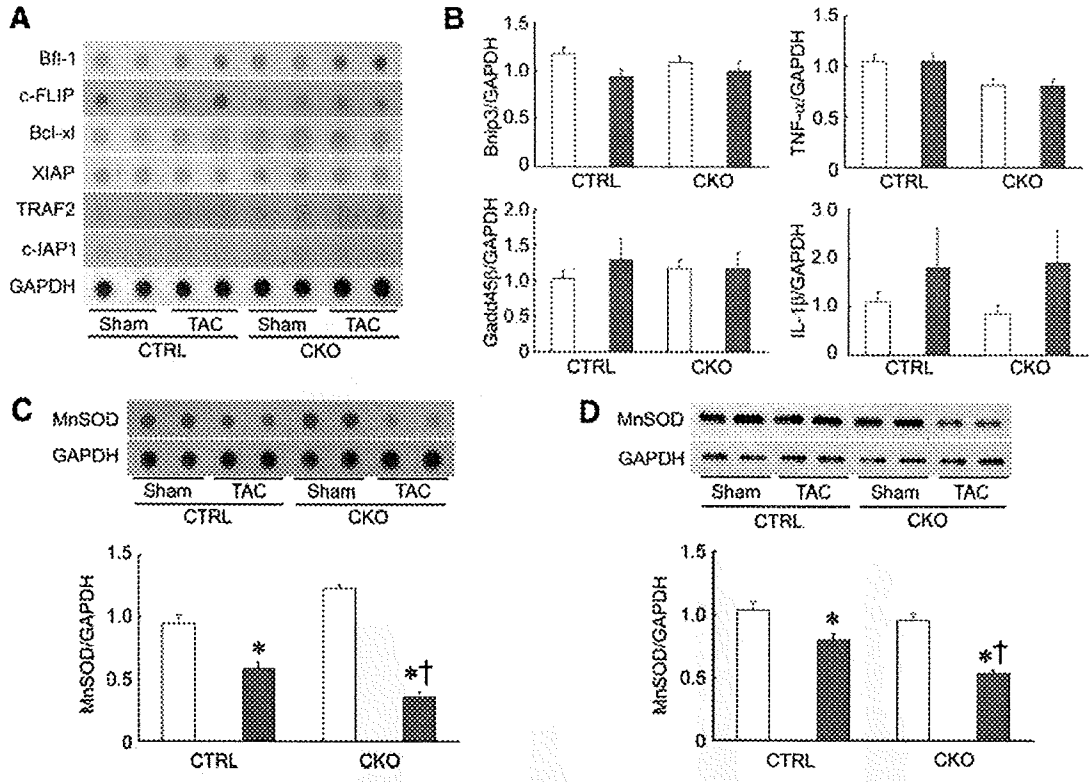

Figure 5. IKKβ-deficient hearts showed downregulation of MnSOD 1 week after TAC. A, Dot blot analysis of NF-κB target antiapoptotic gene expression. The mRNA expression levels of Bfl-1, c-FLIP, Bcl-xl, XIAP, TRAF2, and c-IAP1 were examined. B, The mRNA expression levels of Bnip3, Gadd45β, TNF-α, and IL-1β quantified with real-time RT-PCR (n=4 or 5 in each group). Target gene/GAPDH ratios in a sham-operated CTRL were set equal to 1. C and D, mRNA levels (n=3 to 6 in each group) (C) and protein levels (n=4 in each group) (D) of MnSOD expression and those densitometric analysis. MnSOD/GAPDH ratio in a sham-operated CTRL mouse was set equal to 1. Unfilled and gray bars represent sham- and TAC-operated groups, respectively. *P<0.05 vs corresponding sham-operated mice; †P<0.05 vs TAC-operated CTRL.

CTRL and CKO and subjected the cells to the following treatments: isoproterenol alone, MnTBAP alone, or isoproterenol with MnTBAP. MnTBAP has no effect on the expression level of MnSOD (data not shown). We calculated the percentage of trypan blue–negative cardiomyocytes, as an index of cell viability. Under normal conditions, cell viability was not significantly different between CTRL and CKO cardiomyocytes (Figure 7A). Treatment with MnTBAP alone did not affect the viability of either group. Treatment with isoproterenol decreased the viability of CKO cardiomyocytes to a greater extent than CTRL cardiomyocytes. MnTBAP significantly improved the viability of CKO cardiomyocytes treated with isoproterenol.

We also examined the effect of JNK inhibition on isoproterenol-induced cardiomyocyte death (Figure 7B). Treatment with a JNK inhibitor II alone did not affect the viability in either group. The JNK inhibitor II significantly improved the viability of isoproterenol-treated CKO cardiomyocytes. Thus, downregulation of MnSOD and enhanced activation of JNK are both involved in the increased apoptosis in CKO mice after TAC.

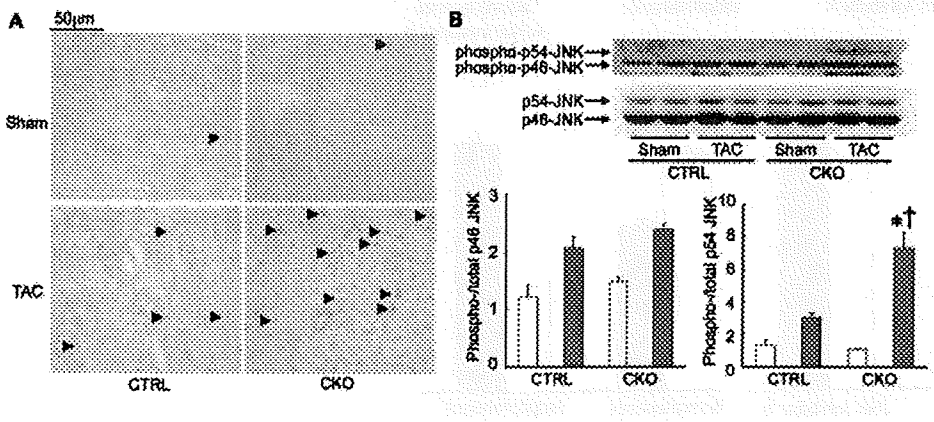

Figure 6. IKKβ-deficient hearts showed enhanced oxidative stress and increased JNK activity 1 week after TAC. A, Immunohistochemical staining with 8-OHdG antibody. Some of 8-OHdG–positive nuclei are indicated by black arrow heads. B, Western blot analysis of phospho- or total JNK and densitometric analysis of these blots (n=2 in sham-operated groups, n=3 in TAC-operated groups). Phospho-/total JNK ratio in a sham-operated CTRL mouse was set equal to 1. Open and gray bars represent sham- and TAC-operated group, respectively. *P<0.05 vs corresponding sham-operated mice; †P<0.05 vs TAC-operated CTRL.

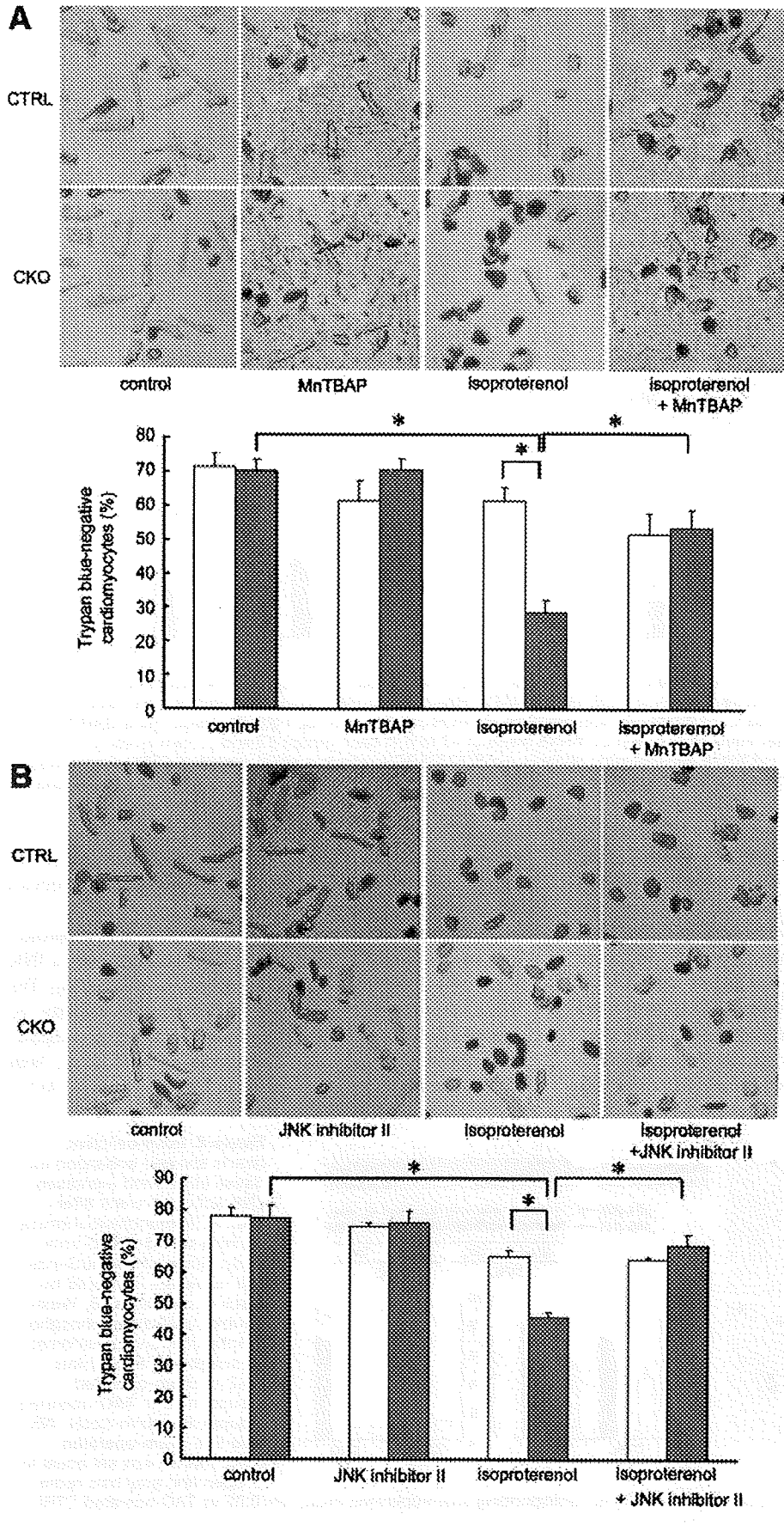

Figure 7. MnSOD mimetic or JNK inhibitor improved the viability of cardiomyocytes isolated from CKO hearts. The effects of MnTBAP (a MnSOD mimetic) (A) or JNK inhibitor II (B) were examined as described in Materials and Methods. Representative images of cardiomyocytes stained with trypan blue and the percentage of trypan blue–negative cardiomyocytes are shown. Open and gray bars represent cardiomyocytes from CTRL and CKO, respectively. *$P<0.05$.

Discussion

In response to pressure overload, the hearts activates an adaptive physiological response in the form of cardiac hypertrophy, whereas long-lasting or excessive exposure to mechanical stress results in transition to heart failure.[20] In the present study, we found that the ablation of IKKβ in cardiomyocytes increased pressure overload–induced cardiomyocyte apoptosis, leading to cardiac dysfunction and chamber dilation. These findings indicate that the acute activation of NF-κB in a setting of pressure overload has protective properties. A protective role of the IKKβ/NF-κB signaling pathway in cardiomyocytes is inconsistent with some of previous studies of p50-deficient mice. The ablation of p50 improved cardiac function and survival after myocardial infarction.[8,9] However, there was paradoxical increase in TNF-α expression in p50-deficient hearts after myocardial infarction, and it is likely that the use of p50-deficient mice to examine the role of NF-κB pathway is problematic. Although there are some alternate complexes of NF-κB, heterodimers of p65 and p50 are the most common activated complexes. However, after prolonged activation of the p65-p50 dimer, NF-κB is converted from the transcriptionally active p65-p50 heterodimer into the transcriptionally inactive p50-p50 homodimer, which acts as a transcriptional repressor.[21] This may be a native negative-feedback mechanism to prevent excessive inflammation. Thus, it is possible that lack of p50-p50 homodimer formation in p50-deficient mice resulted in the paradoxical enhancement of NF-κB activity, which conferred the cardioprotective effects. In addition, Frantz et al also reported that the reduction of cardiac ischemia/reperfusion injury in p50-deficient mice was abolished with transplantation of bone marrow cells isolated from wild-type mice, indicating that the primary mechanism of injury is activation of NF-κB in infiltrating leukocytes and not in cardiomyocytes.[22] Taken together, these observations suggest that p50-deficient mice may not be the appropriate model to clarify the role of the NF-κB pathway in cardiomyocytes. Thus, we used cardiomyocyte-specific IKKβ-deficient mice in this study. We efficiently inhibited activation of both the cardiac IKK complex and NF-κB in response to pressure overload using this model.

The role of the pathway differs among cell types. Enterocyte-specific knockout of IKKβ prevented a systemic inflammation but resulted in severe apoptotic damage to the reperfused intestinal mucosa.[17] In contrast, hepatocyte-specific knockout of IKKβ prevented ischemia/reperfusion-induced necrotic injury in the liver,[23] and neuron-specific knockout of IKKβ significantly ischemia-induced apoptosis of neuron.[24] These findings indicate that in vivo, NF-κB can have different effects on the mechanism of cell death, depending on the organ or type of stimulus.

Here, we found that the IKKβ/NF-κB pathway is a negative regulator of programmed cell death. NF-κB induces the transcriptional activation of antiapoptotic and antioxidant molecules.[25] Quantification of mRNA expression of NF-κB–dependent antiapoptotic genes revealed that MnSOD is responsible for the protective role of NF-κB. MnSOD was severely downregulated in IKKβ-deficient hearts after TAC. Sustained JNK activation, which has been observed in IKKβ- or RelA-deficient cells, promotes apoptosis.[19] JNK activation is mediated by the downregulation of MnSOD, reactive oxygen species accumulation, and resultant inactivation of mitogen-activated protein kinase (MAPK) phosphatase.[19] We observed enhanced oxidative stress and JNK activation in pressure-overloaded hearts of mice. However, we did not measure MAPK phosphatase activity, because it is technically difficult to estimate its specific activity in hearts. Given that the activity of apoptosis signal-regulating kinase 1, which is an upstream kinase of JNK, was not significantly different between control and IKKβ-deficient hearts (data not shown), it is possible that inactivation of MAPK phosphatase is involved in the enhanced JNK activation observed in IKKβ-deficient hearts. Furthermore, we examined whether IKKβ/NF-κB–MnSOD–JNK linkage is associated with the protective mechanism in cardiomyocytes using cardiomyocytes isolated from adult mice. We found that the IKKβ-deficient cardiomyocytes were more susceptible to isoproterenol-induced death and that the susceptibility was attenuated by treatment with either a MnSOD mimetic or a JNK inhibitor. These results indicate that this pathway is a critical component of the cardiomyocyte defense against acute hemodynamic stress. However, we cannot exclude the possibility that other molecules than MnSOD may contribute to increased apoptosis in CKO. In addition, considering that this pathway functions proapoptotic in other organs, the function of NF-κB pathway may be different in the setting of chronic heart failure.

Although the expression of MnSOD decreased in response to pressure overload, the magnitude of the decrease was enhanced in pressure-overloaded IKKβ-deficient hearts. However, the molecular mechanism of the pressure overload–induced downregulation in IKKβ-deficient mice remains to be elucidated. A series of transcription factors, such as specificity protein-1, activator protein-2, CCAAT/enhancer-binding protein, p53, and NF-κB, reportedly regulate MnSOD gene expression.[26–28] Among these factors, activation of NF-κB is essential, but not sufficient, for the induction of MnSOD.[26] In contrast, it is well known that p53 functions as a negative regulator of MnSOD gene transcription and that p53 is induced in response to pressure overload in the heart.[29] NF-κB has been shown to antagonize p53 transactivation through the induction of p53 proteolysis or sequestration of the p300 and CREB-binding protein coactivators.[30,31] Thus, the absence of NF-κB–driven p53 inhibition after TAC might decrease MnSOD in IKKβ-deficient mice.

In conclusion, we demonstrated that IKKβ/NF-κB plays a protective role in the cardiomyocyte response to pressure overload. The IKKβ/NF-κB signaling pathway may constitute a molecular target for the prevention and treatment of heart failure.

Acknowledgments

We are grateful to M. Karin (University of California at San Diego) for the gift of *Ikbk*$\beta^{flox/flox}$ mice and K. Chien (Harvard University) for the gift of *MLC2V-Cre* mice.

Sources of Funding

This work was supported by a Grant-in-Aid for Scientific Research from the Ministry of Education, Culture, Sports, Science and Technology, Japan (to K.O. and S.H.) and from Takeda Science Foundation (to S.H.).

Disclosures

None.

References

1. Yamaguchi O, Higuchi Y, Hirotani S, Kashiwase K, Nakayama H, Hikoso S, Takeda T, Watanabe T, Asahi M, Taniike M, Matsumura Y, Tsujimoto I, Hongo K, Kusakari Y, Kurihara S, Nishida K, Ichijo H, Hori M, Otsu K. Targeted deletion of apoptosis signal-regulating kinase 1 attenuates left ventricular remodeling. *Proc Natl Acad Sci U S A*. 2003; 100:15883–15888.
2. Hikoso S, Yamaguchi O, Higuchi Y, Hirotani S, Takeda T, Kashiwase K, Watanabe T, Taniike M, Tsujimoto I, Asahi M, Matsumura Y, Nishida K, Nakajima H, Akira S, Hori M, Otsu K. Pressure overload induces cardiac dysfunction and dilation in signal transducer and activator of transcription 6-deficient mice. *Circulation*. 2004;110:2631–2637.
3. Wencker D, Chandra M, Nguyen K, Miao W, Garantziotis S, Factor SM, Shirani J, Armstrong RC, Kitsis RN. A mechanistic role for cardiac myocyte apoptosis in heart failure. *J Clin Invest*. 2003;111:1497–1504.
4. Yussman MG, Toyokawa T, Odley A, Lynch RA, Wu G, Colbert MC, Aronow BJ, Lorenz JN, Dorn GW II. Mitochondrial death protein Nix is induced in cardiac hypertrophy and triggers apoptotic cardiomyopathy. *Nat Med*. 2002;8:725–730.
5. Hayden MS, Ghosh S. Signaling to NF-κB. *Genes Dev*. 2004;18: 2195–2224.
6. Hirotani S, Otsu K, Nishida K, Higuchi Y, Morita T, Nakayama H, Yamaguchi O, Mano T, Matsumura Y, Ueno H, Tada M, Hori M. Involvement of nuclear factor-κB and apoptosis signal-regulating kinase 1 in G-protein-coupled receptor agonist-induced cardiomyocyte hypertrophy. *Circulation*. 2002;105:509–515.
7. Higuchi Y, Otsu K, Nishida K, Hirotani S, Nakayama H, Yamaguchi O, Matsumura Y, Ueno H, Tada M, Hori M. Involvement of reactive oxygen species-mediated NF-κB activation in TNF-α-induced cardiomyocyte hypertrophy. *J Mol Cell Cardiol*. 2002;34:233–240.
8. Kawano S, Kubota T, Monden Y, Tsutsumi T, Inoue T, Kawamura N, Tsutsui H, Sunagawa K. Blockade of NF-κB improves cardiac function and survival after myocardial infarction. *Am J Physiol Heart Circ Physiol*. 2006;291:H1337–H1344.
9. Frantz S, Hu K, Bayer B, Gerondakis S, Strotmann J, Adamek A, Ertl G, Bauersachs J. Absence of NF-κB subunit p50 improves heart failure after myocardial infarction. *FASEB J*. 2006;20:1918–1920.
10. Kawamura N, Kubota T, Kawano S, Monden Y, Feldman AM, Tsutsui H, Takeshita A, Sunagawa K. Blockade of NF-κB improves cardiac function and survival without affecting inflammation in TNF-α-induced cardiomyopathy. *Cardiovasc Res*. 2005;66:520–529.
11. O'Donnell SM, Hansberger MW, Connolly JL, Chappell JD, Watson MJ, Pierce JM, Wetzel JD, Han W, Barton ES, Forrest JC, Valyi-Nagy T, Yull FE, Blackwell TS, Rottman JN, Sherry B, Dermody TS. Organ-specific roles for transcription factor NF-κB in reovirus-induced apoptosis and disease. *J Clin Invest*. 2005;115:2341–2350.
12. Li ZW, Omori SA, Labuda T, Karin M, Rickert RC. IKKβ is required for peripheral B cell survival and proliferation. *J Immunol*. 2003:170: 4630–4637.
13. Chen J, Kubalak SW, Minamisawa S, Price RL, Becker KD, Hickey R, Ross J Jr, Chien KR. Selective requirement of myosin light chain 2v in embryonic heart function. *J Biol Chem*. 1998;273:1252–1256.
14. Hikoso S, Ikeda Y, Yamaguchi O, Takeda T, Higuchi Y, Hirotani S, Kashiwase K, Yamada M, Asahi M, Matsumura Y, Nishida K, Matsuzaki M, Hori M, Otsu K. Progression of heart failure was suppressed by inhibition of apoptosis signal-regulating kinase 1 via transcoronary gene transfer. *J Am Coll Cardiol*. 2007;50:453–462.
15. Fujii J, Ikeda Y, Watanabe T, Kawasaki Y, Suzuki K, Fujii C, Takahashi M, Taniguchi N. A defect in the mitochondrial import of mutant Mn-superoxide dismutase produced in Sf21 cells. *J Biochem*. 1998;124: 340–346.
16. Deleted in proof.
17. Chen LW, Egan L, Li ZW, Greten FR, Kagnoff MF, Karin M. The two faces of IKK and NF-κB inhibition: prevention of systemic inflammation but increased local injury following intestinal ischemia-reperfusion. *Nat Med*. 2003;9:575–581.
18. Nakai A, Yamaguchi O, Takeda T, Higuchi Y, Hikoso S, Taniike M, Omiya S, Mizote I, Matsumura Y, Asahi M, Nishida K, Hori M, Mizushima N, Otsu K. The role of autophagy in cardiomyocytes in the basal state and in response to hemodynamic stress. *Nat Med*. 2007;13: 619–624.
19. Kamata H, Honda S, Maeda S, Chang L, Hirata H, Karin M. Reactive oxygen species promote TNFα-induced death and sustained JNK activation by inhibiting MAP kinase phosphatases. *Cell*. 2005;120:649–661.
20. Opie LH, Commerford PJ, Gersh BJ, Pfeffer MA. Controversies in ventricular remodelling. *Lancet*. 2006;367:356–367.
21. Lawrence T, Gilroy DW, Colville-Nash PR, Willoughby DA. Possible new role for NF-κB in the resolution of inflammation. *Nat Med*. 2001: 7:1291–1297.
22. Frantz S, Tillmanns J, Kuhlencordt PJ, Schmidt I, Adamek A, Dienesch C, Thum T, Gerondakis S, Ertl G, Bauersachs J. Tissue-specific effects of the nuclear factor κB subunit p50 on myocardial ischemia-reperfusion injury. *Am J Pathol*. 2007;171:507–512.
23. Luedde T, Assmus U, Wustefeld T, Meyer zu Vilsendorf A, Roskams T, Schmidt-Supprian M, Rajewsky K, Brenner DA, Manns MP, Pasparakis M, Trautwein C. Deletion of IKK2 in hepatocytes does not sensitize these cells to TNF-induced apoptosis but protects from ischemia/reperfusion injury. *J Clin Invest*. 2005;115:849–859.
24. Herrmann O, Baumann B, de Lorenzi R, Muhammad S, Zhang W, Kleesiek J, Malfertheiner M, Kohrmann M, Potrovita I, Maegele I, Beyer C, Burke JR, Hasan MT, Bujard H, Wirth T, Pasparakis M, Schwaninger M. IKK mediates ischemia-induced neuronal death. *Nat Med*. 2005;11: 1322–1329.
25. Dutta J, Fan Y, Gupta N, Fan G, Gelinas C. Current insights into the regulation of programmed cell death by NF-κB. *Oncogene*. 2006;25: 6800–6816.
26. Jones PL, Ping D, Boss JM. Tumor necrosis factor α and interleukin-1β regulate the murine manganese superoxide dismutase gene through a complex intronic enhancer involving C/EBP-β and NF-κB. *Mol Cell Biol*. 1997;17:6970–6981.
27. Dhar SK, Xu Y, Chen Y, St Clair DK. Specificity protein 1-dependent p53-mediated suppression of human manganese superoxide dismutase gene expression. *J Biol Chem*. 2006;281:21698–21709.
28. Darville MI, Ho YS, Eizirik DL. NF-κB is required for cytokine-induced manganese superoxide dismutase expression in insulin-producing cells. *Endocrinology*. 2000;141:153–162.
29. Sano M, Minamino T, Toko H, Miyauchi H, Orimo M, Qin Y, Akazawa H, Tateno K, Kayama Y, Harada M, Shimizu I, Asahara T, Hamada H, Tomita S, Molkentin JD, Zou Y, Komuro I. p53-induced inhibition of Hif-1 causes cardiac dysfunction during pressure overload. *Nature*. 2007: 446:444–448.
30. Vousden KH, Lu X. Live or let die: the cell's response to p53. *Nat Rev Cancer*. 2002;2:594–604.
31. Webster GA, Perkins ND. Transcriptional cross talk between NF-κB and p53. *Mol Cell Biol*. 1999;19:3485–3495.

Advance Publication by J-STAGE

Circulation Journal
Official Journal of the Japanese Circulation Society
http://www.j-circ.or.jp

Enhanced Expression of the S100A8/A9 Complex in Acute Myocardial Infarction Patients

Takashi Katashima, MD; Takahiko Naruko, MD*; Fumio Terasaki, MD; Masatoshi Fujita, MD**; Kaoru Otsuka, MD; Shougo Murakami, MD; Akira Sato, MD†; Michiaki Hiroe, MD††; Yoshihiro Ikura, MD‡; Makiko Ueda, MD‡; Masaki Ikemoto, PhD**; Yasushi Kitaura, MD

Background: S100A8/A9 complex (S100A8/A9) is expressed in activated human neutrophils and macrophages. Enhanced expression of S100A8/A9 in atherosclerotic plaque of patients with unstable angina pectoris (UAP) has been demonstrated, but its profile in acute myocardial infarction (AMI) has not been clarified.

Methods and Results: Serum S100A8/A9 levels were serially measured in patients with AMI (n=55) and UAP (n=16) during the acute period. The expression of S100A8/A9 was examined immunohistochemically in the infarcted myocardium of 7 autopsied patients with AMI. Serum S100A8/A9 levels on the 1st day were 1,118±115 (SE) ng/ml in AMI patients as compared with 787±147 ng/ml in UAP patients. On days 3–5, serum S100A8/A9 levels in AMI patients reached a peak value and were significantly higher than the values in UAP patients (1,690±144 ng/ml vs 844±100 ng/ml; P<0.0001). In AMI patients, peak S100A8/A9 levels positively correlated with peak white blood cell and neutrophil counts, and peak creatine kinase-MB and peak C-reactive protein levels. Double immunostaining revealed that S100A8/A9 was specifically expressed in neutrophils and macrophages infiltrating the infarcted myocardium.

Conclusions: S100A8/A9 is implicated in the pathophysiology of AMI and may be an additional biomarker of the local inflammatory response following AMI.

Key Words: Inflammation; Myocardial infarction; Pathology; Proteins

The S100A8/A9 complex is a heterodimeric molecule of the S100 family and is composed of S100A8 (10.8 kD) and S100A9 (13.2 kD), containing 2 calcium-binding sites per molecule. The 2 subunits are expressed in activated human neutrophils and macrophages in inflammatory lesions. S100A8 and S100A9 noncovalently associate to quickly form a heterodimer, the S100A8/A9 complex.[1] Translocation of the complex from the cytosol to the membrane is induced by activation of a novel pathway requiring an intact microtubule network.[2]

Editorial p???

Recent clinical studies have demonstrated elevated serum levels of the S100A8/A9 complex in inflammatory disorders, such as rheumatoid arthritis,[3] transplant rejection,[4] unstable angina pectoris (UAP),[5] acute myocardial infarction (AMI),[6,7] and recent MI.[8] Overexpression of the S100A8/A9 complex has been shown immunohistochemically in atherosclerotic plaques in coronary and carotid arteries.[5,6,9] High levels of S100A9 in human atherosclerotic rupture-prone lesions are also reported.[10] Furthermore, the mechanistic implication of S100A8/A9 in the pathophysiology of atherosclerosis and vascular inflammation has been demonstrated.[11] Thus, elevated serum S100A8/A9 levels in AMI are attributable to coronary vulnerable plaques.

Meanwhile, it has been reported that activated macrophages infiltrating the myocardial tissue of patients with active cardiac sarcoidosis highly express the S100A8/A9 complex.[12] Although myocardial necrosis is the major histological feature of AMI, it is a well-known fact that inflammatory responses develop in the infarcted myocardium.[13] Neutrophil infiltration is present at the border of the infarct 24 h after symptom onset, and macrophages begin to appear

Received July 31, 2009; revised manuscript received December 19, 2009; accepted December 21, 2009; released online February 27, 2010 Time for primary review: 32 days

Department of Internal Medicine III, Osaka Medical College, Takatsuki, *Department of Cardiology, Osaka City General Hospital, Osaka, **Human Health Sciences, Kyoto University Graduate School of Medicine, Kyoto, †Department of Cardiology, University of Tsukuba Graduate School of Comprehensive Human Science, Tsukuba, ††Department of Cardiology, International Medical Center of Japan, Tokyo and ‡Department of Pathology, Osaka City University Graduate School of Medicine, Osaka, Japan

The first two authors contributed equally to this work.

Mailing address: Fumio Terasaki, MD, Department of Internal Medicine III, Osaka Medical College, 2-7 Daigaku-machi, Takatsuki 569-8686, Japan. E-mail: in3012@poh.osaka-med.ac.jp

ISSN-1346-9843 doi:10.1253/circj.CJ-09-0564

Table 1. Clinical Characteristics of the Patients

Characteristics	AMI (n=55)	UAP (n=16)	P value
Age (years)	66.8±1.4	74.8±1.8	0.005
Sex (M/F)	37/18	10/6	NS
Risk factors			
Hypertension, n (%)	39 (71)	12 (75)	NS
SBP (mmHg)	144.4±3.5	152.8±5.6	NS
DBP (mmHg)	86.9±2.3	82.0±2.6	NS
DM, n (%)	29 (53)	6 (38)	NS
FBS (mg/dl)	115.0±3.6	106.2±3.5	NS
Hypercholesterolemia, n (%)	38 (69)	12 (75)	NS
LDL-cholesterol (mg/dl)	136.6±5.6	135.4±8.6	NS
HDL-cholesterol (mg/dl)	51.2±1.9	47.1±2.2	NS
Triglyceride (mg/dl)	136.0±10.6	151.8±19.0	NS
Smoking, n (%)	12 (22)	3 (19)	NS
BMI (kg/m^2)	23.6±0.4	22.5±0.3	NS
Prior medication			
Aspirin, n (%)	29 (49)	12 (75)	NS
β-blocker, n (%)	12 (22)	5 (31)	NS
ACE inhibitor/ARB, n (%)	31 (56)	10 (63)	NS
Calcium channel blocker, n (%)	19 (35)	9 (56)	NS
Nitrate, n (%)	16 (29)	6 (38)	NS
Statin, n (%)	25 (45)	6 (38)	NS
Laboratory data			
WBC ($\times 10^3/\mu l$)	8.5±0.4	6.8±0.3	0.017
Neutrophils ($\times 10^3/\mu l$)	6.2±0.4	4.5±0.3	0.020
CK-MB (U/L)	44.0±6.9	14.2±2.0	NS
CRP (mg/dl)	5.6±1.6	2.2±0.8	NS
Angiographic findings			
1-vessel disease, n (%)	25 (45)	2 (12)	NS
2-vessel disease, n (%)	21 (38)	8 (50)	NS
3-vessel disease, n (%)	9 (16)	6 (38)	NS
Time from onset of chest pain to first blood draw (h)	4.7±0.5	4.7±1.1	NS
Time from onset of chest pain to PCI (h)	6.0±0.5	7.7±1.1	NS

Values are expressed as the mean±SE.
AMI, acute myocardial infarction; UAP, unstable angina pectoris; NS, not significant; SBP, systolic blood pressure; DBP, diastolic blood pressure; DM, diabetes mellitus; FBS, fasting blood sugar; LDL, low-density lipoprotein; HDL, high-density lipoprotein; BMI, body mass index; ACE, angiotensin-converting enzyme; ARB, angiotensin receptor blocker; WBC, white blood cell; CK-MB, creatine kinase isoenzyme MB fraction; CRP, C-reactive protein; PCI, percutaneous coronary intervention.

in the infarct area 3–5 days after symptom onset. By 1 week after symptom onset, neutrophils have decreased and granulation tissue becomes established with neocapillary invasion, and infiltration of macrophages, lymphocytes, and plasma cells.[13] Therefore, an alternative source of the S100A8/A9 complex may be these inflammatory cells. We hypothesized that the source of the S100A8/A9 complex in AMI may not only be coronary atherosclerotic plaques, but also the infarcted myocardium. Therefore, the purpose of this study was to compare serially measured serum S100A8/A9 levels of patients with AMI, and those of patients with UAP, as well as immunohistochemically examining the expression profile of the S100A8/A9 complex in myocardium obtained from autopsied AMI patients.

Methods

Clinical Studies

The study cohort consisted of 71 patients with either AMI [67±1 (SE) years; 37 men, 18 women] or UAP [75±2 (SE) years; 10 men, 6 women]. AMI was diagnosed on the basis of: (1) chest pain >30 min in duration, (2) ST-segment elevation >0.1 mV in 2 contiguous ECG leads, (3) total or subtotal occlusion of the infarct-related artery, (4) elevated creatine kinase (CK)-MB isoenzyme more than 2-fold within 12 h of chest pain, and (5) successful primary coronary angioplasty (defined as Thrombolysis In Myocardial Infarction flow[15] grade 3 with a residual diameter stenosis <30%). UAP was diagnosed according to Braunwald's criteria.[16] We excluded patients with non-atherosclerotic inflammatory disorders, such as pneumonia and vasculitis, in order to avoid potentially confounding effects with respect to serum levels of the S100A8/A9 complex. A total of 30 healthy volunteers who were free of chronic conditions associated with coronary artery disease, such as hyperlipidemia, hypertension and diabetes, served as controls.

This study complied with the Declaration of Helsinki, and was approved by the institutional review committees of the Osaka Medical College Hospital; the subjects gave informed consent.

Advance Publication by J-STAGE

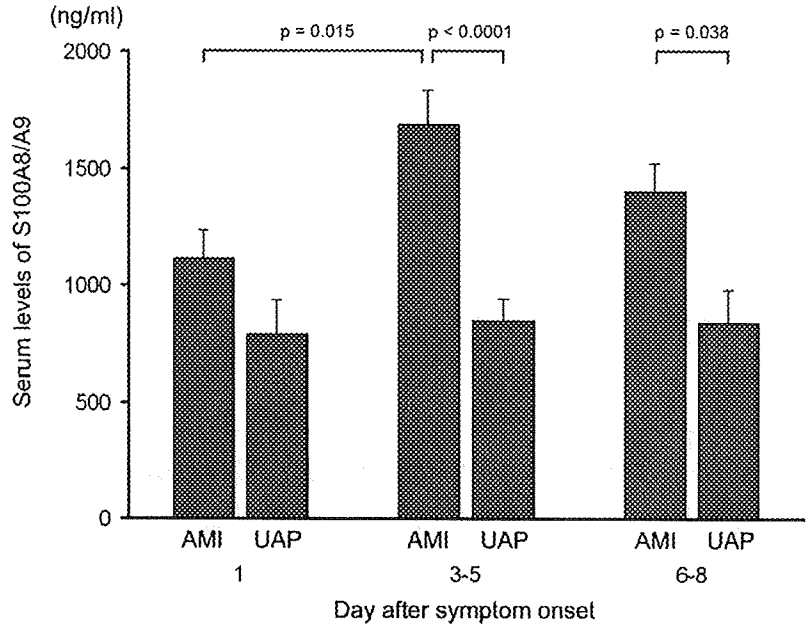

Figure 1. Changes in serum S100A8/A9 complex levels in acute myocardial infarction (AMI) and unstable angina pectoris (UAP) after symptom onset. In AMI patients, serum S100A8/A9 complex levels peaked at 3–5 days after the onset of symptoms and were significantly higher than levels on day 1. Serum S100A8/A9 complex levels in UAP patients remained unchanged until days 6–8 after the onset of symptoms. At both 3–5 days and 6–8 days after the onset of symptoms, serum S100A8/A9 complex levels in AMI patients were significantly higher than those in UAP patients. Red bars: serum S100A8/A9 complex levels in AMI patients; blue bars: serum S100A8/A9 complex levels in UAP patients.

Measurement of Serum Levels of the S100A8/A9 Complex

Serum S100A8/A9 complex levels were serially measured, using a sandwich enzyme-linked immunosorbent assay system that was developed in our laboratory,[4] in patients with AMI and UAP during the acute period [ie, from the time of symptom onset (day 1 of hospitalization) to day 8 of hospitalization]. All AMI and UAP patients underwent successful primary coronary angioplasty within 12h of the onset of symptoms. The first sample was taken prior to revascularization treatment and subsequent samples were taken after treatment in all patients. White blood cell (WBC) counts and serum levels of C-reactive protein (CRP), CK, and CK-MB were measured by conventional methods. Comparison analyses were conducted between serum S100A8/A9 complex levels and other clinical features.

Pathological Studies

Frozen myocardial samples were obtained at autopsy from 7 patients who had died between 1 and 9 days after the onset of AMI. In addition, frozen myocardial samples from individuals who died of non-cardiovascular causes (n=6) served as references. The frozen samples were subsequently serially sectioned at a thickness of 6μm, and fixed in acetone. All first sections were stained with hematoxylin-eosin; the other sections were used for immunohistochemical staining.

Immunohistochemistry

Single Staining The cellular components were analyzed using monoclonal antibodies against macrophages (EBM11; DAKO, Glostrup, Denmark) and neutrophils (CD66b; Beckman Coulter, Fullerton, CA, USA). Commercially available monoclonal antibodies against S100A8 and S100A9 (both from Santa Cruz Biotechnology, Santa Cruz, CA, USA) and a rabbit polyclonal antibody against the S100A8/A9 complex were used to investigate immunolocalization of these protein monomers and complex. The methods of the anti-S100A8/A9 complex antibody production and specificity testing were reported previously.[4] The specificity of the results obtained with these antibodies was checked by omitting the primary antibodies and using non-immune mouse IgG serum (DAKO) and non-immune rabbit serum (DAKO) for monoclonal and polyclonal antibodies, respectively, as negative controls. Sections were incubated at 4°C overnight or 1h at room temperature, and then subjected to a 3-step staining procedure, using the streptavidin–biotin complex method for detection. Peroxidase activity was visualized with 3-amino-9-ethyl-carbazole (10min, room temperature), and the sections were faintly counterstained with hematoxylin.

Table 2. Correlation of Peak Serum S100A8/A9 Complex Levels With Laboratory Variables in Patients With AMI

	r	P value
Peak WBC (×10³/μl)	0.453	0.001
Peak neutrophils (×10³/μl)	0.444	0.002
Peak CK-MB (U/L)	0.307	0.036
Peak CRP (mg/dl)	0.370	0.011

Abbreviations see in Table 1.

Double Immunostaining To identify cell types that stained positive for the S100A8/A9 complex, we also performed double immunostaining for the neutrophil (CD66b)/S100A8/A9 complex and macrophage (CD68)/S100A8/A9 complex, according to the previously described method, with minor procedural modifications.[17] In this staining method, alkaline phosphatase is visualized with fast blue BB (blue, neutrophils or macrophages), and peroxidase is visualized with 3-amino-9-ethyl-carbazole (red, S100A8/A9 complex).

Quantitative Methods The area occupied by S100A8-, S100A9-, and S100A8/A9-complex-positive cells was quantified by computer-aided planimetry, and expressed as a percentage of the myocardial tissue area. The number of CD66b-positive neutrophils was counted and expressed as the number of cells/mm² of myocardial tissue. The macrophage-positive area was quantified and expressed as percent area.

Table 3. Clinical Characteristics of 7 Autopsied Patients With AMI

Case no.	Age/sex	IRA	Interval between symptom onset and death	Risk factors	Cause of death
1	70/M	LAD	6h	Smoking	Cardiac rupture
2	73/F	RCA	1 day	HT, HL, DM, smoking	Cardiac rupture
3	58/M	RCA	2 days	DM, smoking	CHF due to multivessel disease
4	62/M	LMT	2 days	Smoking	CHF
5	79/M	LAD	7 days	HT, smoking	VF
6	69/M	LMT	9 days	Smoking	CHF
7	84/M	LAD	9 days	HT	CHF due to multivessel disease

IRA, infarct-related artery; LAD, left anterior descending coronary artery; RCA, right coronary artery; HT, hypertension; HL, hyperlipidemia; CHF, congestive heart failure; LMT, left main trunk; VF, ventricular fibrillation. Other abbreviations see in Table 1.

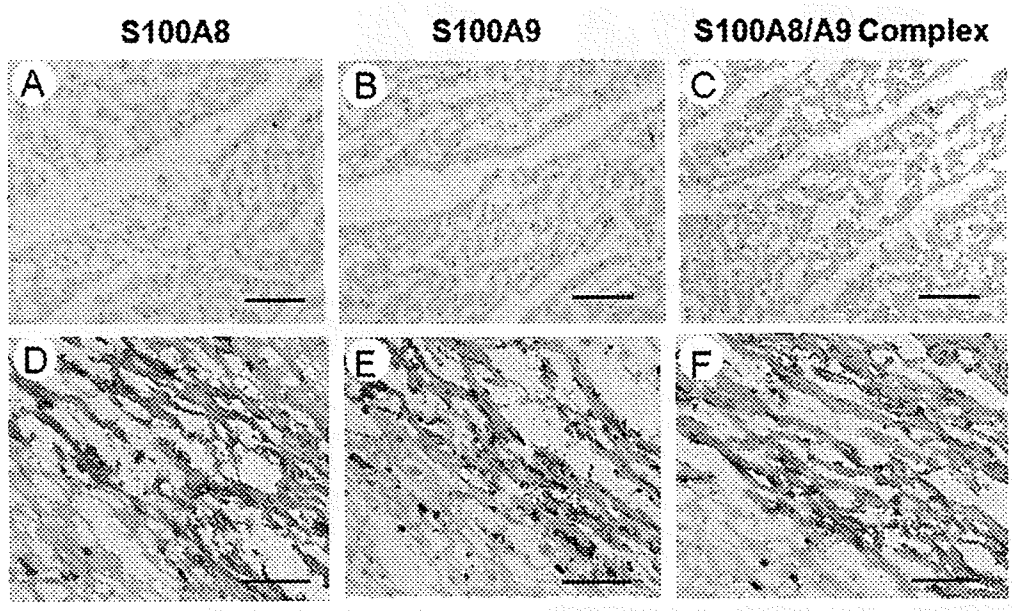

Figure 2. Micrographs showing S100A8-, S100A9-, and S100A8/A9-complex-expression in autopsied human myocardium from a reference case (A–C) and from an AMI patient (D–F). (A,D) Immunostaining for S100A8; (B,E) immunostaining for S100A9; (C,F) immunostaining for S100A8/A9 complex. The anti-S100A8, S100A9, and S100A8/A9-complex antibodies exhibit scattered S100A8-, S100A9-, S100A8/A9-complex-positive cells in the myocardium from a reference case, whereas they show abundant positive cells in the infarcted myocardium from an AMI patient (case 2 in Table 3). Bars=100 μm.

In addition, on the basis of double immunostaining for the neutrophil (CD66b)/S100A8/A9 complex and macrophage (CD68)/S100A8/A9 complex, the percentage of S100A8/A9-complex-positive neutrophils in the total neutrophil count and S100A8/A9-complex-positive macrophages in the total macrophage count were calculated.

Statistical Analysis

Data are presented as the mean±SE. Comparing parameters between 2 groups was performed with the chi-square test or the unpaired 2-tailed Student's t-test. Comparison across more than 2 groups involved 1-way analysis of variance (ANOVA) with Bonferroni correction when appropriate. Serum S100A8/A9 complex levels were compared over time, using repeated measure ANOVA. Pearson's correlation coefficients were used to evaluate the relations between serum S100A8/A9 complex levels and clinical parameters. The morphometric analysis was performed by a single investigator who was unaware of the patients' characteristics and histological classifications. For comparisons of 2 groups of individuals, the Mann-Whitney U test was used in all circumstances. Differences were considered statistically significant at $P<0.05$.

Results

Clinical Information

Clinical features of the 55 AMI and 16 UAP patients on admission are shown in Table 1. The AMI patients were younger than the UAP patients. WBC and neutrophil counts were higher in the AMI patients than in the UAP patients. Otherwise, there were no statistically significant differences between the 2 groups.

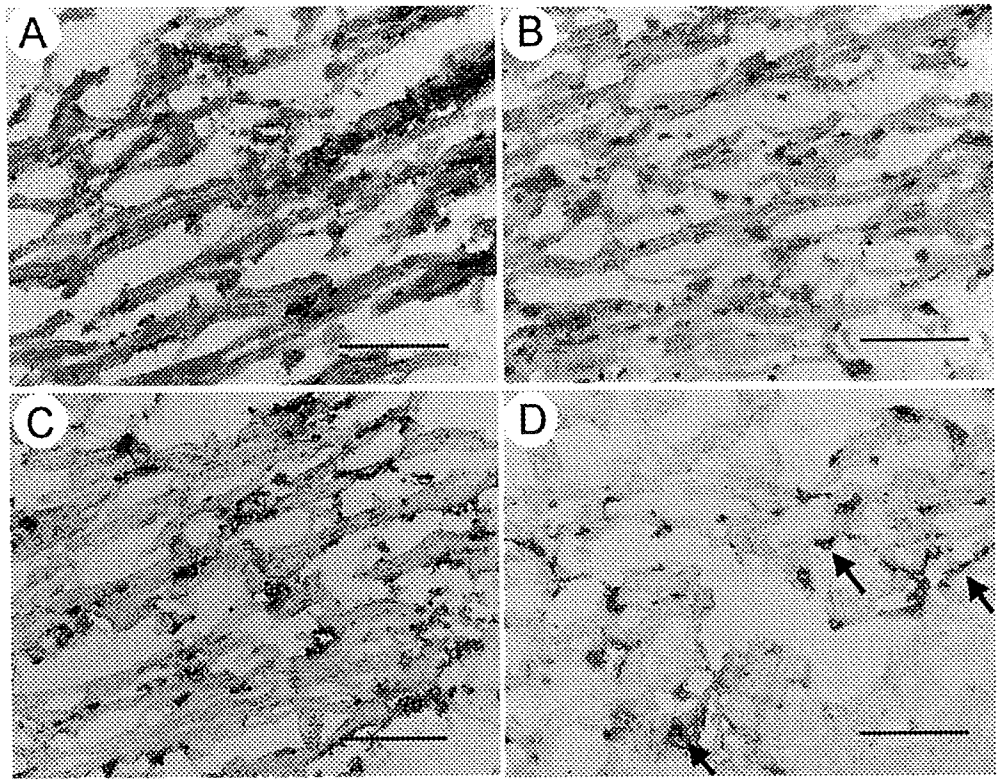

Figure 3. Micrographs of the infarcted myocardium from an autopsied patient (case 3 in **Table 3**). (**A**) Anti-CD66b antibody staining reveals a large number of neutrophils in the infarct area. (**B**) An adjacent section stained with anti-S100A8/A9 complex also reveals the presence of S100A8/A9-complex-positive cells. (**C**) Double immunostaining for CD66b (blue) and the S100A8/A9 complex (red) reveals that most cells show double staining (purple), thus indicating that most S100A8/A9-complex-positive cells are neutrophils. (**D**) Double immunostaining for macrophages (blue) and the S100A8/A9 complex (red) reveals that few cells (arrows) show double staining (purple), thus indicating that few S100A8/A9-complex-positive cells are macrophages. Bars = 100 μm.

Measurement of Serum Levels of the S100A8/A9 Complex

The serum S100A8/A9 complex levels on day 1 of symptom onset were significantly higher in AMI patients than in normal controls [1,118±115 (SE) ng/ml vs 230±21 ng/ml; P< 0.0001], and peaked between days 3 and 5 (1,690±144 ng/ml). In UAP patients, the serum S100A8/A9 complex levels on day 1 of symptom onset were 787±147 ng/ml, which was also significantly higher than that in normal controls (P=0.028). The serum S100A8/A9 complex levels in UAP patients remained unchanged until days 6–8 after symptom onset. On days 3–5, the serum S100A8/A9 complex levels was significantly higher in AMI patients than in UAP patients (1,690± 144 ng/ml vs 844±100 ng/ml; P<0.0001; **Figure 1**). In AMI patients the peak level of S100A8/A9 complex positively correlated with the peak WBC count (r=0.453, P=0.001), peak neutrophil count (r=0.444, P=0.002), peak CK-MB level (r=0.307, P=0.036), and peak CRP level (r=0.370, P=0.011) (**Table 2**).

Pathological Studies

The clinical characteristics of the 7 autopsied patients with AMI are summarized in **Table 3**. Regarding the staining pattern of S100A8, S100A9, and the S100A8/A9 complex, there was no significant difference among the 3 antibodies. The anti-S100A8, S100A9, and S100A8/A9-antibodies showed scattered S100A8-, S100A9-, S100A8/A9-complex-positive cells in the myocardium from the reference cases (**Figures 2A–C**), whereas in the infarcted myocardium of the AMI patients the 3 antibodies showed abundant S100A8, S100A9, and S100A8/A9-complex-positive cells (**Figures 2 D–F**). The S100A8/A9 complex was specifically and strongly positive in neutrophils and macrophages infiltrating the infarcted myocardium of AMI patients. In the early acute phase (from 6 h to 2 days after the onset of AMI), neutrophils were the main component of infiltrating inflammatory cells. Double immunostaining for the S100A8/A9 complex and macrophages or neutrophils showed that the vast majority of S100A8/A9-complex-positive cells were neutrophils at this stage (**Figure 3**). Meanwhile, in the subacute phase (7–9 days after the onset of AMI), the number of accumulating macrophages increased, and double immunostaining showed that most S100A8/A9-complex cells were macrophages in this phase (**Figure 4**).

Quantitative analysis demonstrated that the S100A8-, S100A9-, and S100A8/A9-complex-positive areas were significantly larger (S100A8, P<0.005; S100A9, P<0.005; S100A8/A9 complex, P<0.005) in the infarcted myocardium of AMI patients than in the myocardium from the reference

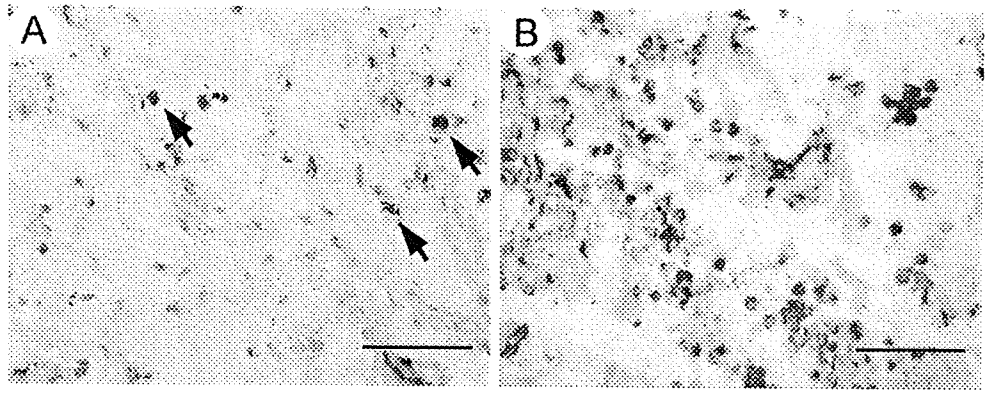

Figure 4. Micrographs of the infarcted myocardium of an autopsied patient (case 7 in Table 3). (A) Double immunostaining for neutrophils (blue) and the S100A8/A9 complex (red) reveals that few cells (arrows) show double staining (purple), thus indicating that few S100A8/A9-complex-positive cells are neutrophils. (B) Double immunostaining for CD68 (blue) and the S100A8/A9 complex (red) reveals that most cells show double staining (purple), thus indicating that, at this stage, most S100A8/A9-complex-positive cells are macrophages. Bars=100 μm.

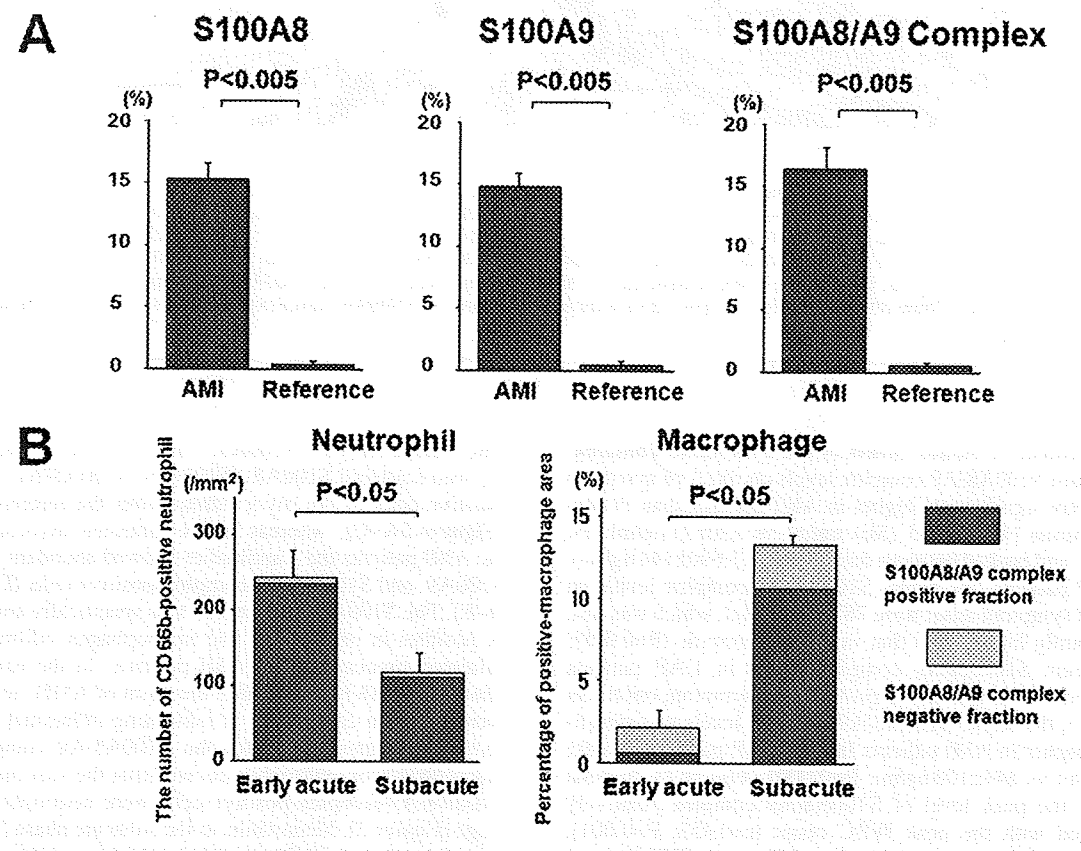

Figure 5. (A) Graphs showing the S100A8-, S100A9-, and S100A8/A9-complex-positive areas expressed as a percentage of the total surface area in autopsied human myocardium from AMI (red bars) and reference cases (grey bars). (B) Graphs showing the number of neutrophils/mm² and the macrophage-positive areas expressed as a percentage of the total surface in the infarcted myocardium in the early acute and subacute phases. Green indicates S100A8/A9-complex-positive fractions. AMI, acute myocardial infarction.

cases (Figure 5A). In the infarcted myocardium of AMI patients, the number of CD66b-positive neutrophils was significantly higher ($P<0.05$) in the early acute phase than in the subacute phase. In contrast, the macrophage-positive area was significantly smaller ($P<0.05$) in the early acute phase than in the subacute phase (Figure 5B). In addition, the percentage of S100A8/A9-complex-positive macrophages in the total macrophage infiltration area was significantly higher in the subacute phase than in the early acute phase (81.0± 3.5% vs 33.0±4.7%, $P<0.05$). In contrast, there was no significant difference between the 2 groups in the percentage of S100A8/A9-complex-positive neutrophils in the total neutrophil number (92.7±1.2% vs 96.3±1.7%, P=NS) (Figure 5B).

Discussion

The novel findings of this study are as follows. First, in AMI patients who had undergone successful primary angioplasty, we showed a transient increase in serum levels of the S100A8/A9 complex with a peak value at 3–5 days after the onset of AMI. Second, we showed a distinct expression of the S100A8/A9 complex in neutrophils and macrophages infiltrating the infarct.

The source of the elevated serum level of the S100A8/A9 complex is attributable to inflammatory lesions in coronary atherosclerotic plaques,[6,18] and in infarcted myocardium, because AMI is associated with both lesions. In the present study, to discriminate the source of the complex, we measured serum levels of the S100A8/A9 complex in patients with UAP, in whom the source of the complex may be limited to coronary vulnerable plaques. Although the serum level remained unchanged for 1 week in UAP patients, in AMI patients it increased by approximately 50% at 3–5 days after the onset of AMI, and showed a still higher level at 6–8 days after the onset, as compared with the baseline value. These findings strongly suggest that serum S100A8/A9 is derived from neutrophils and macrophages infiltrating coronary atherosclerotic plaques and the infarcted area. In previous studies,[6–8] blood concentrations of S100A8/A9 in AMI patients were measured only once, whereas we serially measured the serum levels after the onset of AMI, which lead us to assume the infarcted myocardium was an additional source of the complex.

As an alternate source of S100A8/9 in this setting, circulating leukocytes need to be considered. AMI initiates a systemic response that involves global activation of inflammatory systems. This global activation is partly evidenced by elevated CRP levels and elevated leukocyte counts.[19,20] Thus, it is possible, as an alternate explanation, that the bulk of the circulating S100A8/A9 was derived from the increased numbers of activated circulating neutrophils and macrophages.

Our finding of statistically significant positive correlations between peak serum levels of the S100A8/A9 complex, and peak CK and CK-MB levels indicates that the S100A8/A9 level is largely influenced by infarct size. The level of complex also correlated with peak WBC and CRP levels, thus suggesting that the S100A8/A9 complex is heavily involved in inflammatory disorders. The role of the level of the S100A8/A9 complex in predicting the risk of cardiovascular events has been proposed,[7,8] and it may serve as a biomarker of both the severity and prognosis of AMI.

In the present study, we demonstrated strong expression of the S100A8/A9 complex in the infarcted myocardium of AMI patients, thus suggesting that the S100A8/A9 complex, produced by activated neutrophils and macrophages, is involved in the pathophysiology of AMI. To the best of our knowledge, we are the first to describe the in situ localization of the S100A8/A9 complex in the infarcted myocardium of AMI patients. Regarding the staining pattern of S100A8, S100A9, and the S100A8/A9 complex in the myocardium, there was no significant difference among the 3 antibodies. It has previously been demonstrated in mice and humans that there is heterogeneity in the expression of S100A8, A9, and S100A8/9 complexes by regional macrophages in atherosclerosis.[10,21] However, the expression profile of the monomers and the S100A8/9 complex by leukocytes in infarcted myocardium might be different from that in atherosclerosis.

In the AMI patients, there was a positive correlation between maximal serum levels of the S100A8/A9 complex and maximal blood neutrophil counts in the early acute phase. The circulating neutrophil count reflects activated neutrophils infiltrating the infarcted myocardium and which appear to be a source of S100A8/A9 complex production. Meanwhile, in the subacute phase, the source of S100A8/A9 complex production appeared to be the increased number of activated macrophages in the infarcted myocardium. The shift in the infiltrating inflammatory cells from neutrophils to activated macrophages may reflect the repair of the myocardium by granulation tissue. Enhanced expression of the S100A8/A9 complex in neutrophils and macrophages infiltrating the infarct area may be evidence of the role these phagocytes play in the pathophysiology of AMI.[13] Elucidation of the functional role of the S100A8/A9 complex would aid in the development of future therapeutic strategies for AMI. Further investigations on the mechanistic role of the S100A8/A9 complex are necessary.

Conclusion

Neutrophils and macrophages infiltrating the infarcted myocardium are possibly responsible for the high serum levels of the S100A8/A9 complex found in AMI patients. S100A8/A9 complex may be an additional biomarker of the local inflammatory response following AMI.

Study Limitations

We suggest that the infarcted myocardium is an important source of S100A8/A9 based on prolonged elevation of S100A8/A9 levels following AMI and on the differences in the time course between AMI and UAP. Experiments assessing S100A8/A9 levels in the coronary sinus during coronary intervention and a comparison with peripheral blood levels would provide stronger support for this concept.

Acknowledgment

This study was supported in part by research grants from the Ministry of Health, Labor, and Welfare of Japan (Tokyo, Japan).

Disclosure

Conflict of interest: none declared.

References

1. Roth J, Vogl T, Sorg C, Sunderkotter C. Phagocyte-specific S100 proteins: A novel group of proinflammatory molecules. *Trends Immunol* 2003; **24:** 155–158.
2. Rammes A, Roth J, Goebeler M, Klempt M, Hartmann M, Sorg C. Myeloid-related protein (MRP) 8 and MRP14, calcium-binding proteins of the S100 family, are secreted by activated monocytes via novel, tubulin-dependent pathway. *J Biol Chem* 1997; **272:** 9496–9502.

3. Frosch M, Vogl T, Seeliger S, Wulffraat N, Kuis W, Viemann D, et al. Expression of myeloid-related proteins 8 and 14 in systemic-onset juvenile rheumatoid arthritis. *Arthritis Rheum* 2003; **48:** 2622–2626.
4. Ikemoto M, Tanaka T, Takai Y, Murayama H, Tanaka K, Fujita M. New ELISA system for myeloid-related protein complex (MRP8/14) and its clinical significance as a sensitive marker for inflammatory responses associated with transplant rejection. *Clin Chem* 2003; **49:** 594–600.
5. Miyamoto S, Ueda M, Ikemoto M, Naruko T, Itoh A, Tamaki S, et al. Increased serum levels and expression of S100A8/A9 complex in infiltrated neutrophils in atherosclerotic plaque of unstable angina. *Heart* 2008; **94:** 1002–1007.
6. Altwegg LA, Neidhart M, Hersberger M, Müller S, Eberli FR, Corti R, et al. Myeloid-related protein 8/14 complex is released by monocytes and granulocytes at the site of coronary occlusion: A novel, early, and sensitive marker of acute coronary syndromes. *Eur Heart J* 2007; **28:** 941–948.
7. Healy AM, Pickard MD, Pradhan AD, Wang Y, Chen Z, Croce K, et al. Platelet expression profiling and clinical validation of myeloid-related protein-14 as a novel determinant of cardiovascular events. *Circulation* 2006; **113:** 2278–2284.
8. Morrow DA, Wang Y, Croce K, Sakuma M, Sabatine MS, Gao H, et al. Myeloid-related protein 8/14 and the risk of cardiovascular death or myocardial infarction after an acute coronary syndrome in the Pravastatin or Atorvastatin Evaluation and Infection Therapy: Thrombolysis in Myocardial Infarction (PROVE IT-TIMI 22) trial. *Am Heart J* 2008; **155:** 49–55.
9. McCormick MM, Rahimi F, Bobryshev YV, Gaus K, Zreiqat H, Cai H, et al. S100A8 and S100A9 in human arterial wall: Implications for atherogenesis. *J Biol Chem* 2005; **280:** 41521–41529.
10. Ionita MG, Vink A, Dijike IE, Laman JD, Peeters W, van der Kraak PH, et al. High levels of myeloid-related protein 14 in human atherosclerotic plaques correlate with the characteristics of rupture-prone lesions. *Arterioscler Thromb Vasc Biol* 2009; **29:** 1220–1227.
11. Croce K, Gao H, Wang Y, Mooroka T, Sakuma M, Shi C, et al. Myeloid-related protein-8/14 is critical for the biological response to vascular injury. *Circulation* 2009; **120:** 427–436.
12. Terasaki F, Fujita M, Shimomura H, Tsukada B, Otsuka K, Otsuka K, et al. Enhanced expression of myeloid-related protein complex (MRP8/14) in macrophages and multinucleated giant cells in granulomas of patients with active cardiac sarcoidosis. *Circ J* 2007; **71:** 1545–1550.
13. Frangogiannis NG, Smith CW, Entman ML. The inflammatory response in myocardial infarction. *Cardiovasc Res* 2002; **53:** 31–47.
14. Pathology of myocardial infarction. *In*: Virmani R, Burke A, Farb A, Atkinson JB. Cardiovascular pathology, 2nd edn. Philadelphia: WB Saunders, 2001; 155–178.
15. TIMI Study Group. The Thrombolysis In Myocardial Infarction (TIMI) trial: Phase I findings. *N Engl J Med* 1985; **312:** 932–936.
16. Braunwald E. Unstable angina: A classification. *Circulation* 1989; **80:** 410–414.
17. van der Loos CM, Becker AE, van den Oord JJ. Practical suggestions for successful immunoenzyme double-staining experiments. *Histochem J* 1993; **25:** 1–13.
18. Arakawa K, Yasuda S, Hao H, Kataoka Y, Morii I, Kasahara Y, et al. Significant association between neutrophil aggregation in aspirated thrombus and myocardial damage in patients with ST-segment elevation acute myocardial infarction. *Circ J* 2009; **73:** 139–144.
19. O'Donoghue M, Morrow DA, Cannon CP, Guo W, Murphy SA, Gibson CM, et al. Association between baseline neutrophil count, clopidogrel therapy, and clinical and angiographic outcomes in patients with ST-elevation myocardial infarction receiving fibrinolytic therapy. *Eur Heart J* 2008; **29:** 984–991.
20. Kruk M, Przyluski J, Kalinczuk L, Pregowski J, Deptuch T, Kadziela J, et al. Association of non-specific inflammatory activation with early mortality in patients with ST-elevation acute coronary syndrome treated with primary angioplasty. *Circ J* 2008; **72:** 205–211.
21. Eue I, Langer C, Eckardstein A, Sorg C. Myeloid related protein (MRP) 14 expressing monocytes infiltrate atherosclerotic lesions of ApoE null mice. *Atherosclerosis* 2000; **151:** 593–597.